Microgel emulsion loaded with recombinant oil body as a new drug delivery carrier to promote wound repair

Xinxin Lan
Jilin Agricultural University
Lin Shuangzhu
Affiliated Hospital of Changchun University of Chinese Medicine
Guan Shihui
Affiliated Hospital of Changchun University of Chinese Medicine
Jing Li
Jilin Agricultural University
Weidong Qiang
Jilin Agricultural University
Linna Du
Jilin Agricultural University
Tingting zhou
Jilin Kingmed for Clinical Laboratory Co., Ltd
Yue Dong
Jilin Agricultural University
Xiaokun Li
Jilin Agricultural University
Jing Yang (yangjing5122010@163.com)
Jilin Agricultural University

Research Article

Keywords: Oil body, Oleosin-hEGF, Microgel emulsion, Wound healing.

Posted Date: May 11th, 2022

DOI: https://doi.org/10.21203/rs.3.rs-1631572/v1

Abstract

Background: The skin is an important barrier to protect the body of external damage, there are tens of millions of patients with various skin defects. Due to the complex process of wound repair, it is easy to cause poor healing and other problems. Here, we prepared a new type of transdermal oil body microgel emulsion (OBEME) as a delivery carrier and preliminarily expounded its effect on wound healing.

Method: The basic properties of the OBEME were characterized by scanning electron microscope, cryo-scanning electron microscopy, rheology and thermos- gravimetric analysis. Meanwhile, after 90 d of storage at room temperature, the effects of low-speed centrifugation and repeated freeze-thaw cycles on OBEME were investigated by particle size, potential and fluorescence microscopy tests. Through in vivo transdermal experiments and construction of a full-thickness wound model, the pharmacological effects of OBEME were clarified.

Results: The OBEME is an interconnected network and presents to be smooth with no presence of pores, at the same time, after 90 d of storage at room temperature, the microstructure showed that the oil bodies remained intact. Unaffected by low-speed centrifugation and repeated freeze-thaw cycles. When OBEME treated the mouse skin for 90min, the EGF content in the mouse skin tissue reached the highest, the skin tissue gap was enlarged, and the skin permeability was enhanced. The wound coverage rate exceeded 98 % after treatment for 15 d with OBEME. After OBEME treatment, the inflammatory factor CD68 in the wound tissue was reduced, and the formation of new blood vessels, cytokeratin K5, K19 and collagen was promoted.

Conclusions: The prepared OBEME has good stability, it can alter skin permeability, and promote wound healing by regulating inflammatory response, accelerating angiogenesis, promoting re-epithelialization and remodeling. The OBEME is a new carrier for percutaneous drug delivery, which lays a foundation for the development of new topical drugs.

Introduction

The oil body is a spheroid with a diameter of 0.5–2.5μm, which is an organelle composed of triacylglycerol (TAG) matrix coated into a monolayer of phospholipids and associated protein such as oleosin, caleosin, steroleosin, etc [1–2]. Among them, the acyl hydrophobic part of PL faces TAG, while the hydrophilic part of TA is exposed to the aqueous solution in the cytoplasm, and the oil body protein is embedded in the PL monolayer. Oleosin is composed of three parts: N-terminus, middle hydrophobic region and C-terminus [3]. The intermediate hydrophobic region is inserted into the central domain in TAG, and the N-terminal and C-terminal are exposed outside PL. The foreign protein can be fused to the N or C terminal, and the characteristics of the oil body will not be changed. Oil bodies separate easily, this process eliminates the need for refolding and can reduce the number of chromatography steps to obtain a purified product, thereby reducing consistently the overall cost [4]. Especially, the oil body is similar to liposome, according to this characteristic, the oil body can be used for transdermal drug delivery as a

delivery carrier. For example, oil bodies act as a potential microencapsulation carrier for astaxanthin stabilization and safe delivery [5]. At the same time, based on such a special structure and topological orientation, the oil body can become a new type of drug carrier through genetic engineering technology and expand its application value.

Wound repair is a complex and dynamic process that requires synergistic effect, amongst growth factor, blood cells, transforming growth factor, extracellular matrix etc. When the skin is injured, wound healing begins immediately and consists of several overlapping stages: hemostasis, inflammation, proliferation, and remodeling [6]. EGF may be one of the most well-characterized growth factors affecting skin wound healing [7]. However, the half-life of EGF is too short to show effective biological activity in the treatment of wound [8]. In the preliminary study, we established an oil body expression system, in which the acid fibroblast growth factor (aFGF), basic fibroblast growth factor (bFGF), epidermal growth factor (EGF) and keratinocyte growth factor-2 (KGF2) were expressed on the surface of oil body [9–13]. However, the oil body is not stable in vitro and easy to aggregate [14], which limits the application after separation. Therefore, it is very crucial to maintain the stabilization of oil body in vitro. We selected xanthan gum as the most suitable stabilizer from a variety of compounds [15]. Xanthan gum is a new generation of polysaccharides, which was reported by the United States Drug Administration (USDA) for food and drug use [16]. Because the oil body and xanthan gum have similar types of charges, a mixture of them can cause electrostatic deposition and steric repulsion, so it doesn't aggregate [17], so we prepared oil body microgel emulsion with xanthan gum (OBEME). Microgel is an intramolecular crosslinked polymer chain with the ability of swelling and maintaining a large amount of solvent, and has high water content, large specific surface area and internal network structure which can be used in drug delivery system [18]. In addition, microgels usually contain high-density functional groups, which help to combine with other functional molecules. The ability of internal network structure and biomolecule coupling makes microgel have great application potential in drug delivery system and other biomedical fields [19]. Most importantly, the high porosity and rich functional groups of the microgel facilitate the slow release of the drug. So, we prepared evaluated the characteristic of oil body microgel emulsion with xanthan gum (OBEME) by investigating its micromorphology, rheological properties and thermogravimetric stability. The stability of the OBEME with different storage time, low-speed centrifugation and repeated freezing and thawing was investigated by detecting particle size, potential and microstructure etc. The transdermal properties and the repair efficacy of the OBEME in wound healing were evaluated by immune- hybridization, immunohistochemistry and immunofluorescence methods. The characteristics and pharmacological effects of the microgel emulsion loaded with recombinant oil body as a new drug delivery carrier were preliminarily clarified.

Materials And Methods

Experimental materials and animals

The homozygous transgenic safflower seed was grown in Jilin Agricultural University. In the early stage of our laboratory, the recombinant plasmid pOTB-hEGF-hEGF was constructed. The recombinant plasmid

was transformed into competent cells of Agrobacterium tumefaciens, and the cotyledon nodes were transformed by Agrobacterium-mediated method to obtain transgenic safflower plants. Relatively high expression was identified at the molecular and protein level. The Sprague-Dawley rats (200–220 g) were bought from Beijing HFK Bioscience Co., Ltd. (Beijing, China). The animals were fed according to the "license for the use of laboratory animals" of Jilin Agricultural University (SYJK 2018-0023). The rats were fed in a constant environment with a temperature of 25℃ for 12 h and alternating light and darkness, and they were to drink and eat freely. All animal experiments were performed under approving guidelines.

Preparation of the OBEME

The transgenic and wild type safflower seeds (each 200 g) were immersed in 1 L of distilled water respectively for washing according to the method of Qiang et al [13]. The seeds were placed in 2 L of PBS buffer (Monad Biotech Co., Ltd, Wuhan, China) and ground in a colloid mill (Weihai Taifu Xima Motor Co., Ltd, JB/T9542-1999) for 3 min. The extraction procedures of oil body were referred to the methods of Qiang et al [13]. A portion of the oil body was stored and observed at 37℃, room temperature and 4℃. The xanthan gum (Xi an Taihua Pharmaceutical Co. LTD, China) was swollen in water for 24 h to prepare aqueous solution. The oil body suspension of 40%, 60%, 80% (W/V) and xanthan gum solution of 0.3%, 0.4%, 0.5% (W/V) were mixed.

Characterization of the OBEME

The OBEME micromorphology was observed by XL-30 fifield scanning electron microscope (SEM, HITACHI, Japan) and cryo-scanning electron microscope (ZEISS Sigma 300 VP, Germany). The rheology of the OBEME was measured by an optical micro-rheometer (diffusion spectrometer, DWS RheoLab, Switzerland) and performed the measurement according to the instructions, as follows: valid test frequency range 0.1-10M Hz, elastic range 1 Pa-50 KPa, extended frequency range ω= 0.1–10^5 rad/s, and record the sample's storage modulus (G ', stable moduli), frequency (Hz), and loss modulus (G", lost moduli). Differential scanning calorimetry (DSC) was used to measure the thermal properties of the OBEME. The sample was heated from 30 ℃ to 600 ℃ in air at a constant rate of 10℃/min. Thermal weightlessness of the OBEME was evaluated by thermal analyzer (TG, Pyris Diamond). Record the thermal weightlessness curve of the sample.

Stability of the OBEME

The stability of the OBEME was evaluated under freeze-thaw cycle, low-speed centrifugation and different storage time. The OBEME was frozen at -20 ℃ for 22 h, then thawed in a constant temperature water bath at 30 ℃ for 2 hours. Its physical properties were tested after two freeze-thaw cycles. The physical properties of the OBEME were tested after low-speed centrifugation of 3000rpm/min, 4000rpm/min and 5000rpm/min, respectively. Finally, its characteristics of the OBEME were tested at 15 days, 30 days, 60 days and 90 days after storage at room temperature.

Physical properties and microstructure of the OBEME

The particle size and zeta potential of the OBEME were measured using Malvern Mastersizer Nano ZS90 (Malvern Instrument Co., Ltd., UK) after diluting the OBEME into single droplets [15]. The viscosity was detected by a viscometer (Brookfield DV2TLV, USA) at shear rate of 40 1/s and 100 rpm rotation speed. The microstructure was observed according to the method of Lu et al [20]. The OBEME was diluted (OBEME: PBS = 1:50) and placed on a glass slide by FITC (1%, w/v) and Rhodamine (0.1%, w/v) staining. The photos were presented using a laser confocal microscope (IX71, Olympus, Japan).

Transdermal absorption

Thirty female mice (ICR, 20–22 g, Yisi experimental animal technology company, China) were randomly divided into three groups (n = 15/each group). The mice were narcotized with 5% chloral hydrate solution (0.7 mL/100 g). The hair of backside was depilated and smooth skin was exposed. An effective dose of 1μg/cm^2 hEGF in the OBEME was as a sample treatment [9]. The normal skin was as a blank control. The area of treatment was taken 2 cm^2, and the tissue was collected after transdermal delivery of 10 min ~ 90 mins. The collected skin was embedded in paraffin, which were incubated with primary antibody (rabbit anti-hEGF, Bioss, bs-4568R, China) and secondary antibody (goat anti-rabbit IgG SD3003, Celnovte), and then were stained with Diaminobenzidine(DAB) substrate kit (Celnovte, China). The protein was extracted from the collected skin, and analyzed by western blot. The structure of skin tissue was observed by scanning electron microscope (SEM, HITACHI, Japan).

Wound healing assay

The SD rats were randomly divided into 4 groups (n = 18 each group). Full-thickness excision circular wounds of diameter 1.5 cm were created after anesthesia by 5% chloral hydrate. The wounds were treated using different medication, as follows: NaCl as a negative control; xanthan gum as a negative control; wild type oil body microgel emulsion as a negative control, the OBEME as a sample treatment. The effective dose of hEGF was 1μg/ cm^2. Wound healing in all treatment was photographed at 0th day, 5th day, 10th day 15th day and the images were collected and analyzed using software Image J. The healing rates were measured and calculated. Wound healing rate = (initial wound area - final wound area) / initial wound area ×100% [13].

Histopathology, immunohistochemistry and immunofluorescence

The new regenerative skin tissue on 5th day, 10th day 15th day was fixed in 4% paraformaldehyde, dehydrated, embedded in paraffin, sectioned and placed on the slide and stained with hematoxylin and eosin (H&E). The other slices were operated by immunohistochemistry and immunofluorescence. They were blocked with normal goat serum for 1 h and incubated with a primary antibody and secondary antibody (zf-0311, Sp-9001, Beijing Zhongshan Jinqiao Biotechnology Co., Ltd.). The primary antibodies included CD31 (BA2966, Boster, China); CD 68 (BA3638, Boster, China); cytokeratin 5 (bs-1060R, Bioss, China); cytokeratin 19 (bs-2190R, Bioss, China); collagen I (bs-0578R, Bioss, China); collagen III (bs-0549R, Bioss, China); α-SMA (bm-0002, Boster, China). The images were collected using an optical

microscope (BX51T-PHD-J11, Olympus, Japan) and fluorescence inverted microscope (IX71, Olympus, Japan). The mean immunohistochemical staining intensity and fluorescent intensity were calculated via Image V.6.0.

Western blot detection

The total proteins were extracted from the skin tissues using the total protein extraction kit (Solarbio company, China). The extracted total protein was mixed with loading buffer and boiled for 10 min. A sample containing 60 μg of total proteins was loaded on a 12% polyacrylamide gels. The gel was transferred to a polyvinylidene fluoride (PVDF) membrane for 60 min. Subsequently, PVDF membrane was blocked with 5% skimmed milk for 120 min and incubated by primary antibody which is the same to immunohistochemistry and immunofluorescence. The images were taken and counted by Image-Pro plus.

Statistical analysis

All results were statistically counted by means of significant ± SD and analyzed by means of one-way variance (ANOVA). The significant differences were noted for *P < 0.05, **P < 0.01 and *** P < 0.001.

Results

Preparation and characterization of the OBEME

The oil body was destroyed after putting 7 days at 37℃ and triacylglycerol began to be released. Triacylglycerol began to be released after 14 days of storage at 25℃. When the oil body was left in place for 14 days at 4℃, it has decomposed (Fig. 1a). Therefore, the oil body couldn't exist stably in vitro and was difficult to store even at low temperatures. It is very necessary to choose suitable stabilizer in order to maintain stability. In the previous study, we found that xanthan gum could be used as a stabilizer to stabilize oil body [15]. The ratio of oil body and xanthan gum was optimized by potential and particle size analysis. When the oil body content was 80%, the particle size and potential of the OBEME increased by the rise of xanthan gum content. When the oil body content was 40%, 50%, 60%, the particle size first decreased and then increased, while the potential first increased and then decreased (Fig. 1B). The optimal ratio of oil body and xanthan gum in the OBEME was 60% and 0.4% by regression analysis. At this time, the OBEME's potential was − 41.2 mV and the particle size was 803 nm (Fig. 1b). The oil body was wrapped by xanthan gum and showed red spherical structure under the fluorescence microscope, while the oil body showed black spherical cavities by staining with rhodamine and xanthan gum combines with rhodamine to form red (Fig. 1c). The surface of oil body is rich in oleosin which is a hydrophobic basic protein with amphiphilic N-and C-terminal regions [21–23], so the ends of oleosin are not reductive and cannot form complex with rhodamine. The OBEME was round by labeling with FITC, indicating that the structure was complete (Fig. 1c).

By observing the microstructure of the OBEME and xanthan gum under SEM and Cry-SEM, it was found that the xanthan gum exhibited three-dimensional network structure with presence of porous architecture

and the OBEME was smooth with no presence of pores. The OBEME showed a highly interconnected network of presence on the surface (Fig. 1d), the oil body was filled into the pores formed by the xanthan gum and the shape of the oil body didn't change. In addition, according to the rheological test of the OBEME, the elastic modulus (G') and viscosity modulus (G") of the OBEME increased with the increase of shear frequency, but, G" was lower than G' (Fig. 1e). It indicates that the OBEME was a viscous solution system and had a certain frequency dependence. Further shear stress showed that G' decreased with the increase of shear rate, while viscosity modulus (G") first increased and then decreased in the experimental range (Fig. 1f). In the process of increasing shear stress, G' and G" intersection point (G' = G") were the transformation points of phase, the OBEME changed to viscous fluid at this time. Subsequently, the OBEME was subjected to thermogravimetric test to determine the content of physically adsorbed water. In TG thermogram, three decomposition stages have been observed, first is from 40 to 100℃, which is connected with the dehydration process. On the other hand, it was found that an endothermic event was observed in 87.52 ℃ referring to water vaporization (ΔH = 509.789 J g-1), which agreed with the TG curves of the OBEME (Fig. 1g). It describes that this event occurs due to the OBEME dehydration. The second stage starts at about 250 ℃, which is corresponding to the thermal decomposition of xanthan gum. Finally, the temperature from 350 ℃ to 500 ℃ may be caused by the decomposition of oil bodies. By crosslinking the oil body with xanthan gum, the relaxation of the network was prevented when the heat starts to degrade (Fig. 1g). Therefore, the OBEME enhances the stability to heat.

The stability of the OBEME

After 90 days storage at room temperature, the OBEME remained white and uniform in appearance and was spherical and uniform in size by rhodamine dilution (Fig. 2a). Meanwhile, the particle size of the OBEME maintained at 718.56 nm ~ 803.2 nm, the potential was − 37.46 mV ~ -39.9 mV, and the viscosity was within the range of 725 cP-875 cP in different storage time (Fig. 2b, 2c). The oleosin-hEGF fusion proteins in the OBEME didn't degrade after 90 days storage (Fig. 2d). The above results showed that the OBEME remained stable after storage of 90 days. The OBEME had no stratification under different centrifugal force and remained stable, however, the oil body suspension liquid was stratified, the upper layer was oil body, layer and the lower layer was the liquid layer (Fig. 2e). The diluted the OBEME was uniform in size and dispersed uniformly by observing the microstructure of the OBEME after different centrifugal force (Fig. 2f). At different centrifugal force, the particle size of the OBEME maintained at 693.63 nm ~ 731.8 nm, the potential kept − 38.54 mV~ -39.4 mV, and the viscosity of the OBEME has no significant difference (Fig. 2g, 2h). Therefore, there was no effect on the OBEME at low-speed centrifugation. On the other hand, when the OBEME was subjected to treatment of freeze-thaw cycles, its appearance remained unchanged after two freeze-thaw treatments at -20 ℃ (Fig. 2i). The microstructure of the OBEME had no obvious change and kept complete red spherical structures and dispersed evenly (Fig. 2i). At low temperature, the addition of xanthan gum can protect the structure of oleosin to a certain extent and weaken the damage degree of protein structure by ice crystal [22–24]. After freeze-thaw cycles, the target band of oleosin-hEGF fusion proteins in the OBEME was not degraded by SDS-PAGE electrophoresis (Fig. 2j). The particle size, potential and viscosity had no significant change after

repeated freeze-thaw cycles (Fig. 2k, 2l). Therefore, the properties of the OBEME didn't change after freeze-thaw treatment.

Evaluation on trasdermal absorption of the OBEME

The number of positive cells stained in the skin by treatment of the OBEME was significantly higher than that in the control group. And, over time, it penetrates from the epidermis to the basal layer and into the dermis at 90 min (Fig. 3a). The number of positive cells treated by OBEME increased with the extension of treatment time and was the most at 90min (Fig. 3B) and the expression of hEGF protein after treatment of OBEME accumulated with the increase of treatment time by western-blot analysis (Fig. 3C, 3D). The skin tissue appeared voids and the structure became loose after the OBEME treatment, while the control group was very dense by observing the structure of the skin tissue (Fig. 3E). This implies that the OBEME can alter the skin's permeability, allowing it to penetrate into skin tissue, possibly because its hydrophilic functional groups can improve skin hydration [23], thus enhancing the permeability of the OBEME.

Effects of the OBEME on skin wound healing

The granulation tissue can reflect the excellent condition of wound healing [24], and the proliferation of fibroblasts and the formation of new blood vessels were signs of maturation of granulation tissue [25]. The effect of the OBEME was investigated on wound healing of full-thickness cutting models. The wounds of physiological saline and xanthan gum treatment exuded fluid without scabbing on the 5th day. The wounds of wild oil body emulsion and the OBEME treatment groups were scabbed without exudates (Fig. 4a), the granulation had formed and epidermis began to re-epithelize, and the blood vessels and more fibroblasts appeared on the 5th day (Fig. 4b). On the 10th day, the wound of physiological saline, xanthan gum and wild oil body emulsion groups produced scabs. The scabs had fallen off and there were a lot of renascent skin formation in the OBEME treatment group (Fig. 4a). The OBEME was the earliest to form the epidermal layer, and then gradually became thinner as well as the dermis gradually thickened as time went on (Fig. 4b). Another linchpin challenge for skin wound healing is the regeneration of skin affixtures such as hair follicles [26]. The hair follicles structures appeared in wild oil body emulsion and the OBEME groups on the 10th day (Fig. 4b). The hair follicle structure treated physiological saline and xanthan gum began to appear on the 15th day. In the meantime, the more collagen neatly arranged under the epidermis after the OBEME treatment. In each treatment group, the wound area was decreased significantly (Fig. 4c) and the healing rate increased gradually within 15 days (Fig. 4d).

Regulation of the OBEME on inflammatory cytokines

When tissues are injured, an inflammatory response is induced, and pro-inflammatory macrophages increase, leading to postpone the process of wound healing [27]. The pro-inflammatory factors CD68 was expressed in the wound tissue. The content of CD68 in the OBEME treatment group was lower than that in other groups during the wound healing process by immunohistochemical staining (Fig. 5a). The relative expression of CD68 in the OBEME group was only 0.6 times of that in NaCl group on the 5th day

by statistical analysis of immunohistochemistry (Fig. 5c) and the CD68 expression was significantly decreased in the OBEME treatment group as compared with that in other groups by western blot analysis (Fig. 5b, 5d). On the 15th day, the relative expression of CD68 in each treatment group was reduced, and the CD68 in the OBEME treatment group had the most significant reduction (Fig. 5c, 5d). The OBEME could reduce the production of pro-inflammatory factors CD68, shorten the inflammatory process and accelerate wound healing.

The OBEME promotes vascular regeneration

Normal wound healing requires angiogenesis in the newly formed dermis [28]. The CD31 as a biomarker of vascular endothelial cells in blood vessels, was detected in the process of wound healing by immunohistochemistry and western blot. A large number of new vessels were observed at the wound bed in the OBEME groups (Fig. 6a, c). However, only a few expressions of CD31 were found in the control group (Fig. 6a). The expression of CD31 in the OBEME treatment group had higher on the 5th day compared with the control group by western blot (Fig. 6b, d) and peaked on the 10th day, whereafter, began to declined, and the expression was better than the control group. Angiogenesis in new tissues were promoted by the OBEME.

The OBEME promotes epidermal re-epithelialization

Keratin is essential to wound healing for the initiation, maintenance, and completion of epithelialization [29]. Re-epithelialization starts at 24 h after skin injury and continues to increase and turn into remodeling stages of wound healing. The K5 and K19, which are biomarker for basal keratinocytes cell and hair follicle stem cells, and their staining strength increased with the prolongation of healing time (Fig. 7a, 7c). Compared with the control group, K5 protein in the new skin of the OBEME group began to accumulate in the epidermal layer on the 5th day. The expression of K5 was active on the 10th day, and was extended to the 15th day (Fig. 7c,7g. The expression of K5 protein in newborn tissues also gradually increased (Fig. 7d, 7h). In addition, the K19 was found in the basal layer of epidermis and around the hair follicles of accessory organs (Fig. 7a). The expression of K19 in the OBEME group was significantly increased on the 10th day, and continued to increase until the 15th day, as compared with the control group (Fig. 7b,7e,7f). The K19 protein may regulate the proliferation, differentiation and migration of epidermal stem cells, thus promoting wound regeneration and repair.

The OBEME promates the growth of injured skin in remodeling

The synthesis of extracellular matrix (ECM) is also very important in the process of wound healing. The collagen as the main structural and functional protein of ECM, determines the process of wound healing and the reconstruction of physiological function of healing tissue to a great extent [30]. The collagen in skin tissue mainly includes type I (COLI) and type III (COLIII). The COLI was detected in dermis of the OBEME treatment group and the number of COL1 was more than that of the control group (Fig. 8a, e). The expression of COL1 increased gradually, peaked on the 10th day, and then began to decline as the skin remodeling process accelerated (Fig. 8b, f). The expression of COL III gradually increased in new

tissues (Fig. 8c, 8g). The expression of COL III in the OBEME group was higher than that in the control group at all time points, and reached a peak at the 15th day (Fig. 8d, 8h). The increase of COL I and COL III after the OBEME treatment resulted in faster and stronger skin repair. In addition, myofibroblast is the main cell component of granulation tissue which promotes wound healing. Alpha-smooth muscle actin (α-SMA) as a characteristic contractile product expressed during the differentiation of fibroblasts into myofibroblasts, and involved in wound repair and healing [31]. The content of α-SMA in the OBEME treatment group was higher than that in other groups on the 5th and 10th day by immunofluorescence (Fig. 8i), however, the number of α-SMA on the 15th day was lower than that the 10th day. On the contrary, the number of α-SMA in the control group increased continuously on the 15th day (Fig. 8J). The α-SMA in wild type oil body microgel emulsion group also had a downward trend on the 15th day (Fig. 8K), however, the expression level of α-SMA in the OBEME was the lowest. The expression of α-SMA was significantly decreased in the OBEME group as compared with that in other groups on the 15th day by gray value of western blot (Fig. 8l). In general, the content of α-SMA increased, that is, more myofibroblasts were formed. It can secrete a large number of bioactive substances, such as fibronectin and collagen, which is also an inevitable process of wound healing [32].

Discussion

In the plant seed, phospholipids and amphiphilic oleosin on the surface of oil body to stabilize the organelles, and oleosins prevent the oil body from gathering by steric hindrance [33–34]. The mixed surface membrane is adsorbed around triglyceride core, which is mainly two layers, one layer was considered to be composed of a primary mixed layer of phospholipids and oleosin, and a secondary layer was germ protein. Among them, a germ protein plays an important role in the long-term stabilization of oil body against assembling [14]. Therefore, the oil body is stable in the seed for a long time. However, we found that the oil body ruptured after being stored in vitro for a period of time. This may be due to the lack of germ protein in the separate oil body or the interactions, which lead to the formation of droplet networks and its rearrangement took place at a relatively high rate, leading to instability [14, 35]. Therefore, xanthan gum is chosen as the matrix, which is participate in the process of wound healing [36–37]. Xanthan gum can be enriched in the external surface of adjacent oil body and interacted with each other to protect the stability of oil body, which may form bridge flocculation with oil body through hydrophobic bonding. The repulsive steric force is enhanced by the interaction of oil and xanthan gum, which in turn forms hydrogen bonds and makes it more resistant to external forces. Based on this, it may be the reason why the OBEME has good stability. In addition, xanthan gum is able to increase the temperature range of decomposition and the formed rate of volatile decomposition products during heating was slow [38].

Water gradually forms ice crystals at low temperature, and oil droplets are close to each other in the unfrozen water phase, which may lead to the fracture of the interface layer and promote the accumulation of oil droplets [39]. However, xanthan gum is a polyhydroxy compound with very strong water absorption and strong water retention in the composite system, so that the free water in the composite system is less, reducing the generation of ice crystals [39]. On the other hand, the protein

around the lipid droplets is thick and forms a protective layer that prevents ice formation, fat crystallization, interfacial phase transitions, and biopolymer conformations. So, the OBEME prepared with xanthan gum as a matrix maintained high stability after freeze-thaw cycles.

The oil body linked hEGF has better transdermal absorption effect, hEGF accumulation in the skin was the highest at 60min and decreased at 90min, indicating that hEGF had been released [13]. However, hEGF accumulation in skin tissue was the highest after treated with the OBEME for 90min, which significantly improved its sustained release effect. It may be due to the fact that the OBEME is a storable microgel that distributes drug molecules in the inner layer or specific regions of the microgel through self-assembly or hydrophilic interactions. In addition, the oil body is rich in oleic acid, which is commonly used as a permeation promoter and may play a role in transdermal penetration. On the other hand, the structure of the oil body is similar to that of liposomes, which increases the permeability of the skin to embedded drugs [40]. Its diameter was smaller, which is conducive to transdermal absorption and the skin treated by the OBEME can deliver the drug more effectively through the stratum corneum into the deeper layer. The xanthan gum as the excipient had the slow-release effect for example, the floating chitosan-xanthan beads were used to control the release of glipizide [41]. Because the skin tissue has a highly hydrated water environment, which the OBEME is more easily permeated into the skin than oil body. Xanthan gum has the characteristics of improving the biodistribution of drugs, prolonging the half-life of drugs, and protecting drugs from degradation in the microenvironment. Therefore, it blocks the possibility of EGF being degraded by proteases. As a transdermal drug, skin toxicity is also very important. In previous studies, it was proved that OBEME has non-irritating and sensitizing effects, and showing good safety [42].

Wound healing is a complex biological process, involving inflammation, re-epithelialization and tissue remodeling [43]. When tissues are injured, the pathogen are released, resulting in complex inflammatory response. A large number of macrophage precursors are recruited, which affect the speed of wound healing. However, the OBEME effectively covered the wound, removed exudates, and reduced the expression of macrophage marker CD68. It may be related to the fact that the OBEME is rich in unsaturated fatty acids such as oleic acid and linoleic acid, which can inhibit inflammatory factors [44], thereby shortening the inflammatory period of the wound after the OBEME treatment. On the other hand, EGF regulates early inflammatory response to promote wound re-epithelialization [45]. The OBEME promoted the expression of CD31 and K5 and K19 and thus accelerated angiogenesis and epithelialization. In the proliferative phase, the wound is repaired by the proliferation and migration of epithelial cells, fibroblasts and vascular endothelial cells. In the later period of healing, the quantity, thickness and density of collagen were changing all the time. Collagen is rich in COLIII, which plays an essential role in the formation of new capillaries [46]. COL1 is a protein in the ECM, which acts as a structural scaffold in tissues. Collagen can increase the density of covalent cross-linking and cross-linking with non-collagen components. So, the increase of collagen contributes to the rapid healing of wounds [13]. In the remodeling phase, the OBEME enhanced the expression of COLI and COLIII, thus providing structural integrity for new tissues. In the proliferative phase, the increase of myofibroblasts by up-regulation α-SMA is helpful to reduce the wound area, however, with the prolongation of wound

healing time, α-SMA expression level directly affects the degree of tissue fibrosis. The expression of α-SMA was down-regulated on day 15, suggesting that the decrease of α-SMA expression level could reduce the trend of scar formation and improve the quality of wound repair.

Conclusion

Here, a novel transdermal delivery carrier the OBEME was prepared, which was composed of 0.4 (w/w) xanthan gum and 60% (w/w) oil body. The OBEME has a porous structure and a smooth surface. The addition of xanthan gum increases thermo-oxidative stability and the water absorbing capacity. The OBEME was not affected by repeated freezing and thawing at low temperature and low speed centrifugation, which not only had good stability, but also had the function of accelerating wound healing. It mainly promoted the formation of new blood vessels, inhibited inflammatory response and increased collagen complex to promote the wound repair after skin injury in adult rats. This will provide support for the role of new transdermal drug delivery carriers in wound repair therapy, and also lay the foundation for accelerating the development of new drugs.

Abbreviations

hEGF
human epidermal growth factor
EGF
epidermal growth factor
OBEME
oil body-linked oleosin-hEGF microgel emulsion
CD68
scavenger receptor class D member 1
CD31
platelet endothelial cell adhesion molecule-1
K5
cytokeratin5
K19
cytokeratin19
COLI
Collagen type I
COLIII
Collagen type III
α-SMA
alpha-smooth muscle actin
FITC
fluorescein isothiocyanate

HE
hematoxylin-eosin.

Declarations

Ethics approval and consent to participate

All procedures used in the experiments were complied with the guidelines of the National Ethics Committee on Animal Welfare of China and were approved by the Jilin Agricultural University (SYJK 2018-0023).

Consent for publication

All authors agree to be published.

Availability of data and materials

The datasets used and/or analyzed in the current study are available from the corresponding author on reasonable request.

Conflict of interest

The authors declare that they have no conflict of interest.

Funding:

This work was supported by the Jilin Province Development and Reform Commission [Grant number, 2020C036-2].

Authors' contribution

XXL performed most of the experiments and prepared the draft. JL participated in the measurement of particle size and potential data. LSZ, GSH, WDQ embellished the language. LND and TTZ observed of pathological sections. JY conceived the idea and provided scientific research funds. XKL provided help and consultations. All authors approved the final content.

Acknowledgments

The authors thank for help of Jinnan Guo, Tingting Gao, Yaying Li, Yongxin Guo, Lixia Li, Chang Jia, Sinan Deng, Yilin Liu in the experiment.

References

1. Huang, Ah C. Oil Bodies and Oleosins in Seeds. Annu.rev.plant.Physiol.plant Mol biol. 2003; 43(1):177–200.

2. Siloto, Mp R. The Accumulation of Oleosins Determines the Size of Seed Oilbodies in Arabidopsis. The Plant Cell. 2006; 18(8):1961–1974.
3. Beaudoin F, Wilkinson BM, Stirling CJ, Napier A. In vivo targeting of a sunflower oil body protein in yeast secretory (sec) mutants. Plant Journal for Cell & Molecular Biology. 2010; 23(2):159–170.
4. Acevedo F, Rubilar M, I Jofré, et al. Oil bodies as a potential microencapsulation carrier for astaxanthin stabilisation and safe delivery. Journal of Microencapsulation. 2014;31(5):488–500.
5. Apuano FC, Chimeric oil bodies as an alternative delivery system for peptide vaccines. Università Degli Studi Della Tuscia Viterbo. 2007;25:203–206.
6. Greaves NS, Ashcroft KJ, Baguneid M, Bayat A. Current understanding of molecular and cellular mechanisms in fibroplasia and angiogenesis during acute wound healing. Journal of Dermatological Science. 2013;72(3):206–217.
7. Barrientos S, Stojadinovic O, Golinko MS, Brem H. Tomic-Canic M. Growth factors and cytokines in wound healing. Wound Repair & Regeneration. 2010; 16(5):585–601.
8. Gang G, Li X, Ye X, Qi J, Fan R, Xiang G, Wu Y, Zhou L, A Tong EGF and curcumin co-encapsulated nanoparticle/hydrogel system as potent skin regeneration agent. International Journal of Nanomedicine. 2016;11:3993–4009.
9. Jing Y, Li G, Yong G, et al. Expression of biologically recombinant human acidic fibroblast growth factor in Arabidopsis thaliana seeds via oleosin fusion technology. Gene. 2015;566(1):89–94.
10. Yang J, Qiang W, Ren S, et al. High-efficiency production of bioactive oleosin-basic fibroblast growth factor in A. thaliana and evaluation of wound healing. Gene. 2017; S0378111917307989.
11. Huang J, Yang J, Guan L, et al. Expression of bioactive recombinant human fibroblast growth factor 10 in Carthamus tinctorius L. seeds. Protein Expression & Purification. 2015;7.
12. Qiang W, Gao T, Lan X, et al. Molecular Pharming of the Recombinant Protein hEGF-hEGF Concatenated with Oleosin Using Transgenic Arabidopsis. Genes. 2020; 11:959–972.
13. Qiang W, Zhou T, Lan X, et al. A new nanoscale transdermal drug delivery system: oil body-linked oleosin-hEGF improves skin regeneration to accelerate wound healing. Journal of Nanobiotechnology. 2018; 16.
14. Nikiforidis CV, Kiosseoglou V. Physicochemical stability of maize germ oil body emulsions as influenced by oil body surface-xanthan gum interactions. Journal of Agricultural & Food Chemistry. 2010;58(1):527.
15. Lan X, Qiang W, Yang Y, et al. Physicochemical stability of safflower oil body emulsions during food processing. LWT- Food Science and Technology, 2020, 132(2):109838.
16. Urlacher B, Noble O. Xanthan gum. Thickening & Gelling Agents for Food. 1997;172:202–226.
17. Chen B, Mcclements DJ, Gray DA, Decker EA. Stabilization of soybean oil bodies by enzyme (laccase) cross-linking of adsorbed beet pectin coatings. Journal of Agricultural & Food Chemistry. 2010;58:9259–9265.

18. Wang P, Yang, Q, Zhao C. Molecular Design and Intelligent Material Construction of Light-Responsive Microgel. Progress in Chemistry. 2017.
19. Kumar ML, Rather H, Kedaria D, Rajesh V. Polymeric microgels for bone tissue engineering applications – a review. International Journal of Polymeric Materials. 2020;69(17):381–397.
20. Lu Y, Chi M, Li L, et al, Genome-Wide Identification, Expression Profiling, and Functional Validation of Oleosin Gene Family in Carthamus tinctorius L. Frontiers in plant science. 2018.
21. Chanamai R, Mcclements DJ. Depletion Flocculation of Beverage Emulsions by Gum Arabic and Modified Starch. Journal of Food Science. 2010;66(3):457–463.
22. Aee LH, Hie KN, Nishinari K. DSC and rheological studies of the effects of sucrose on the gelatinization and retrogradation of acorn starch. Thermochimica Acta. 1998;322(1):39–46.
23. Sabino F, Hermes O, Egli FE, Kockmann T, Keller U. In vivo assessment of protease dynamics in cutaneous wound healing by degradomics analysis of porcine wound exudates. Molecular & Cellular Proteomics. 2015;14:354.
24. Yong P. L, Xin Z, Tianli H. Adhesive hemostatic conducting injectable composite hydrogels with sustained drug release and photothermal antibacterial activity to promote full-thickness skin regeneration during wound healing. Small. 2019;15: 12.
25. Thu HE, Zulfakar M, H, Ng SF. Alginate based bilayer hydrocolloid films as potential slow-release modern wound dressing. Int J Pharmaceut. 2012;434:375–383.
26. Zhang Y, Chang M, Bao F, et al. Multifunctional Zn doped hollow mesoporous silica/polycaprolactone electrospun membranes with enhanced hair follicle regeneration and antibacterial activity for wound healing. Nanoscale. 2019.
27. Palaniraj A, Jayaraman V. Production, recovery and applications of xanthan gum by Xanthomonas campestris. Journal of Food Engineering. 2011;106(1):1–12.
28. Lloyd LL, Kennedy JF, Methacanon P, Paterson M, Knill CJ. Carbohydrate polymers as wound management aids. Carbohydrate Polymers. 1998;37(3):315–322.
29. Korting HC, Sch?Llmann C, White RJ. Management of minor acute cutaneous wounds: importance of wound healing in a moist environment. J Eur Acad Dermatol Venereol. 2011;25(2):130–137.
30. Torres P, Díaz J, Arce M. The salivary peptide histatin-1 promotes endothelial cell adhesion, migration, and angiogenesis. The FASEB Journal. 2017;31(11).
31. Bruen KJ, Campbell CA, Schooler WG, Deserres S, Cairns BA, Hultman CS, Meyer AA, Randell SH. Real-time monitoring of keratin 5 expression during burn re-epithelialization. Journal of Surgical Research. 2004;120(1):12.
32. Nath RK, Parks WC, Mackinnon SE, Hunter DA, Markham H, Weeks PM. The regulation of collagen in fetal skin wounds: mRNA localization and analysis. Journal of Pediatric Surgery. 1994;29(7):855–862.
33. Arora PD, McCulloch CA. Dependence of collagen remodelling on alpha-smooth muscle actin expression by fibroblasts. Journal of Cellular Physiology. 1994; 159(1):161.

34. Ghahary A, Shen YJ, Nedelec B, Scott PG, Tredget EE. Enhanced expression of mRNA for insulin-like growth factor-1 in post-burn hypertrophic scar tissue and its fibrogenic role by dermal fibroblasts. Molecular and Cellular Biochemistry. 1995; 148(1):25–32.
35. Tzen JT, Surface structure and properties of plant seed oil bodies. Journal of Cell Biology. 1992;117(2):327–335.
36. Gao ZM, Wang JM, W u NN, Wan ZL, Guo J, Yang XQ, Yin SW. Formation of Complex Interface and Stability of Oil-in-Water (O/W) Emulsion Prepared by Soy Lipophilic Protein Nanoparticles. J Agric Food Chem. 2013; 61(32):7838–7847.
37. Tzen JTC, Lie GC, Huang AHC. Characterization of the charged components and their topology on the surface of plant seed oil bodies. Journal of Biological Chemistry. 1992;267(22):15626.
38. Raschip IE, Hitruc GE, Vasile C, Popescu MC. Effect of the lignin type on the morphology and thermal properties of the xanthan/lignin hydrogels. International Journal of Biological Macromolecules. 2013,54:230–237.
39. Rungnaphar P, Suwapat S. Influence of xanthan gum on rheological properties and freeze–thaw stability of tapioca starch. Journal of Food Engineering. 2008; 88(1):137–143.
40. Marinkovic SS. Liposomes as Drug Delivery Systems in Dermal and Transdermal Drug Delivery. Springer Berlin Heidelberg. 2016.15–38.
41. Kulkarni N, Wakte P, Naik J. Development of floating chitosan-xanthan beads for oral controlled release of glipizide. Int J Pharm Investig. 2015;5(2):73–80.
42. Lan X, Zhou T, Dong Y, et al. Dermal toxicity, dermal irritation and delayed contact sensitization evaluation of oil body linked oleosin-hEGF microgel emulsion via transdermal drug delivery for wound healing. Cutaneous and Ocular Toxicology. 2021;1–25.
43. Junhui Z, Xupin J, Ling f. Involvement of autophagy in hypoxia-BNIP3 signaling to promote epidermal keratinocyte migration. Cell Death & Disease. 2019; 10(3):234.
44. Cardoso CR, Favoreto S, Oliveira LL, Vancim JO, Barban GB, Ferraz DB, Silva JS. Oleic acid modulation of the immune response in wound healing: A new approach for skin repair. Immunobiology. 2011; 216(3):409–415.
45. Kurschat P, Bielenberg D, Rossignol-Tallandier M, Stahl A, Klagsbrun M, Neuron restrictive silencer factor NRSF/REST is a transcriptional repressor of neuropilin-1 and diminishes the ability of semaphorin 3A to inhibit keratinocyte migration. Journal of Biological Chemistry. 2006;281(5):2721–9.
46. Hiramatsu M, Hatakeyama K, Minami N, Kumegawa M. Increase in collagen synthesis of cotton pellet granuloma in rats by epidermal growth factor. The Japanese Journal of Pharmacology. 1982;32(1):198–201

Figures

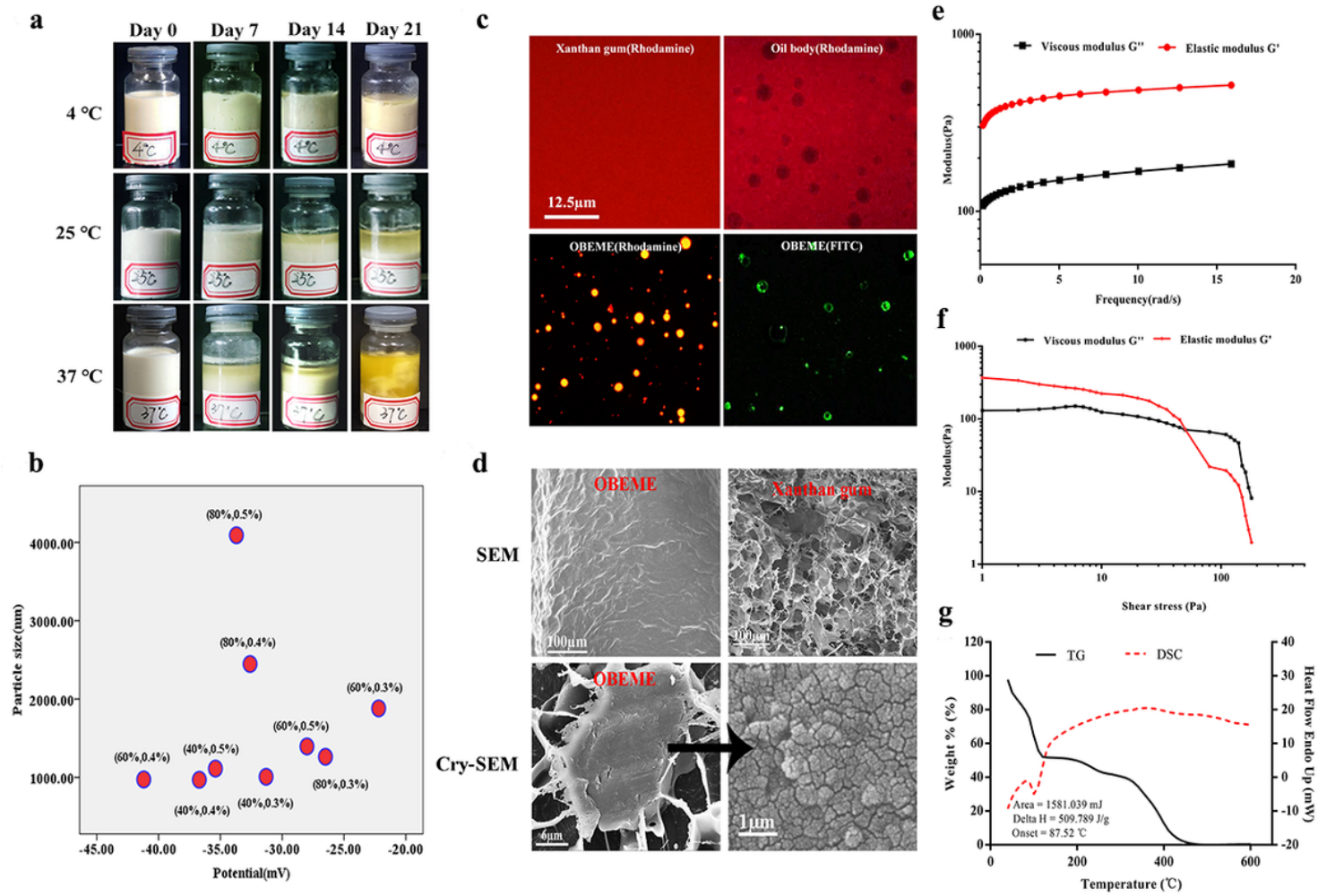

Figure 1

Preparation and characteristic of OBEME. **a** The appearance of oil body stored at 4 °C, 25 °C and 37 °C for 0, 7, 14 and 21 days. **b** The compositional optimization of OBEME. **c** The microstructure of oil body and OBEME labeled with rhodamine and FITC. **d** The SEM and Cry-SEM microstructure of OBEME. **e** Frequency sweep analysis of OBEME. **f** Shear stress analysis of OBEME. **g** TG and DSC analysis of OBEME.

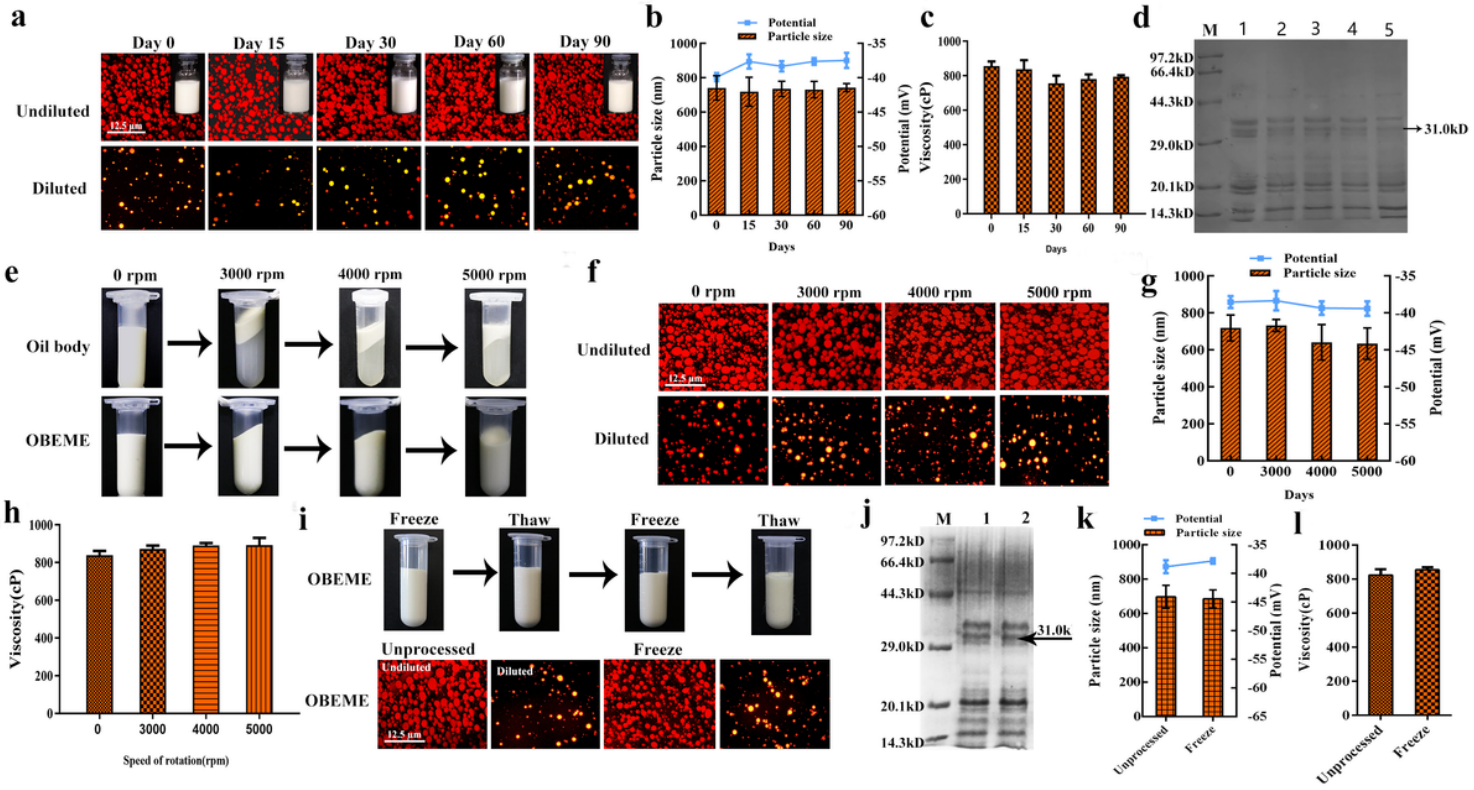

Figure 2

The stability of the OBEME. **a** The appearance and microstructure of OBEME within 90 days; **b** The changes of potential and particle size of OBEME within 90 days; **c** The viscosity change of OBEME within 90 days; **d** Oleosin-hEGF fusion protein analysis in OBEME within 90 days by SDS-PAGE; **e** Appearance of the oil body and the OBEME at different centrifugal speeds; F: Microstructure of the OBEME at different centrifugal speeds; **g** Changes of potential and particle size of the OBEME at different centrifugal speeds; **h** Viscosity changes of the OBEME at different centrifugal speeds; **i** Appearance and microstructure of the OBEME after freeze-thaw cycles; **j** Oleosin-hEGF fusion protein analysis of the OBEME after freeze-thaw cycles by SDS-PAGE; **k** Changes of the OBEME particle size and potential after freeze-thaw cycles; **l** Viscosity changes of the OBEME after freeze-thaw cycles. Compared with the control group, *p<0.05, **p<0.01, ***p<0.001 (n=3) unpaired one-way ANOVA multiple test was used in analyses. bar: 12.5 μm.

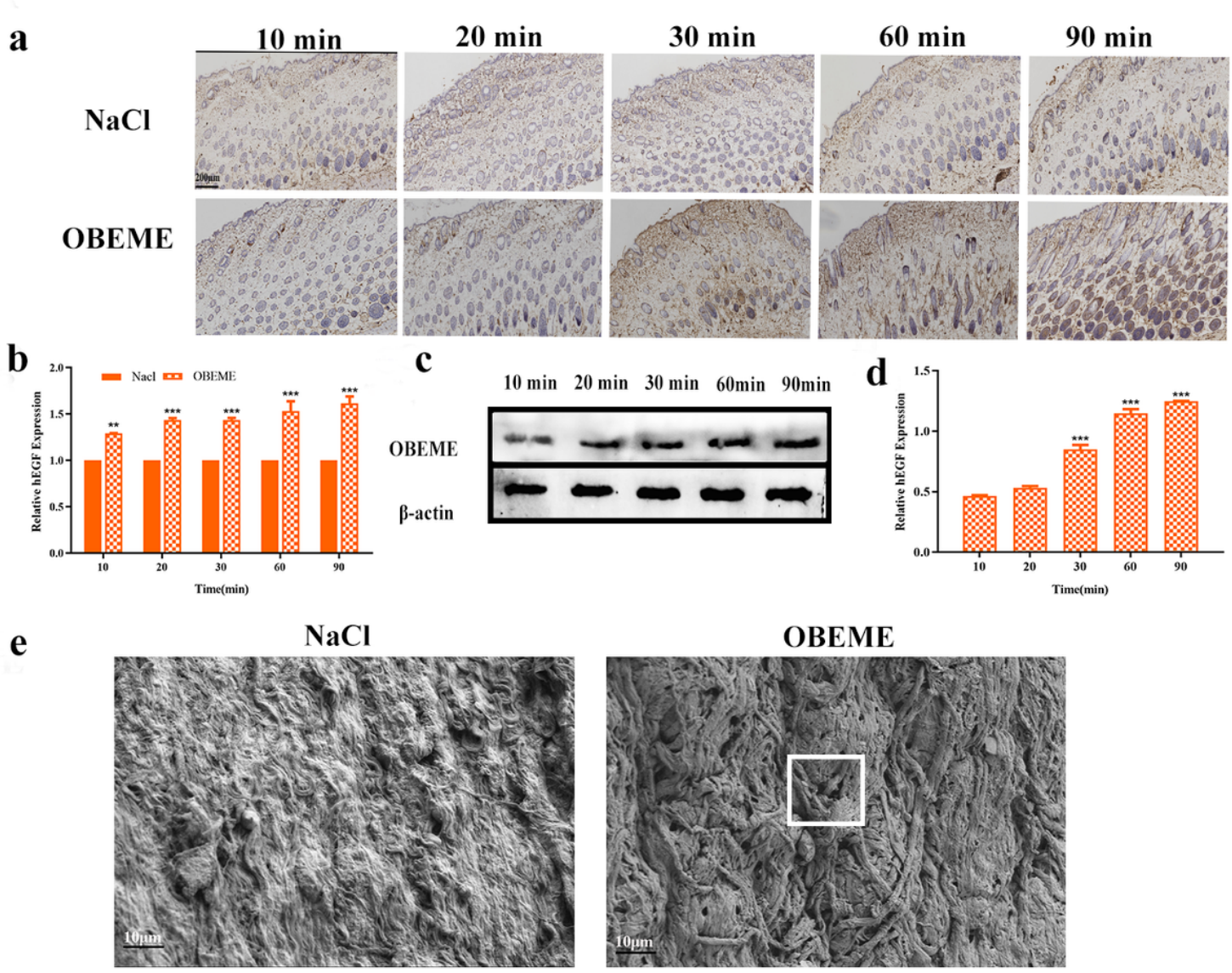

Figure 3

The ability of transdermal absorption of the OBEME. **a** The evaluation of absorption into skin at different times by immunohistochemistry; **b** Statistical analysis of immunohistochemistry; **c** The evaluation of absorption into skin at different times by western blot; **d** Statistical analysis of western blot; **e** SEM of skin. *p<0.05, **p<0.01, ***p<0.001 (n=3). unpaired one-way ANOVA multiple test was used in analyses. bar: 50 μm.

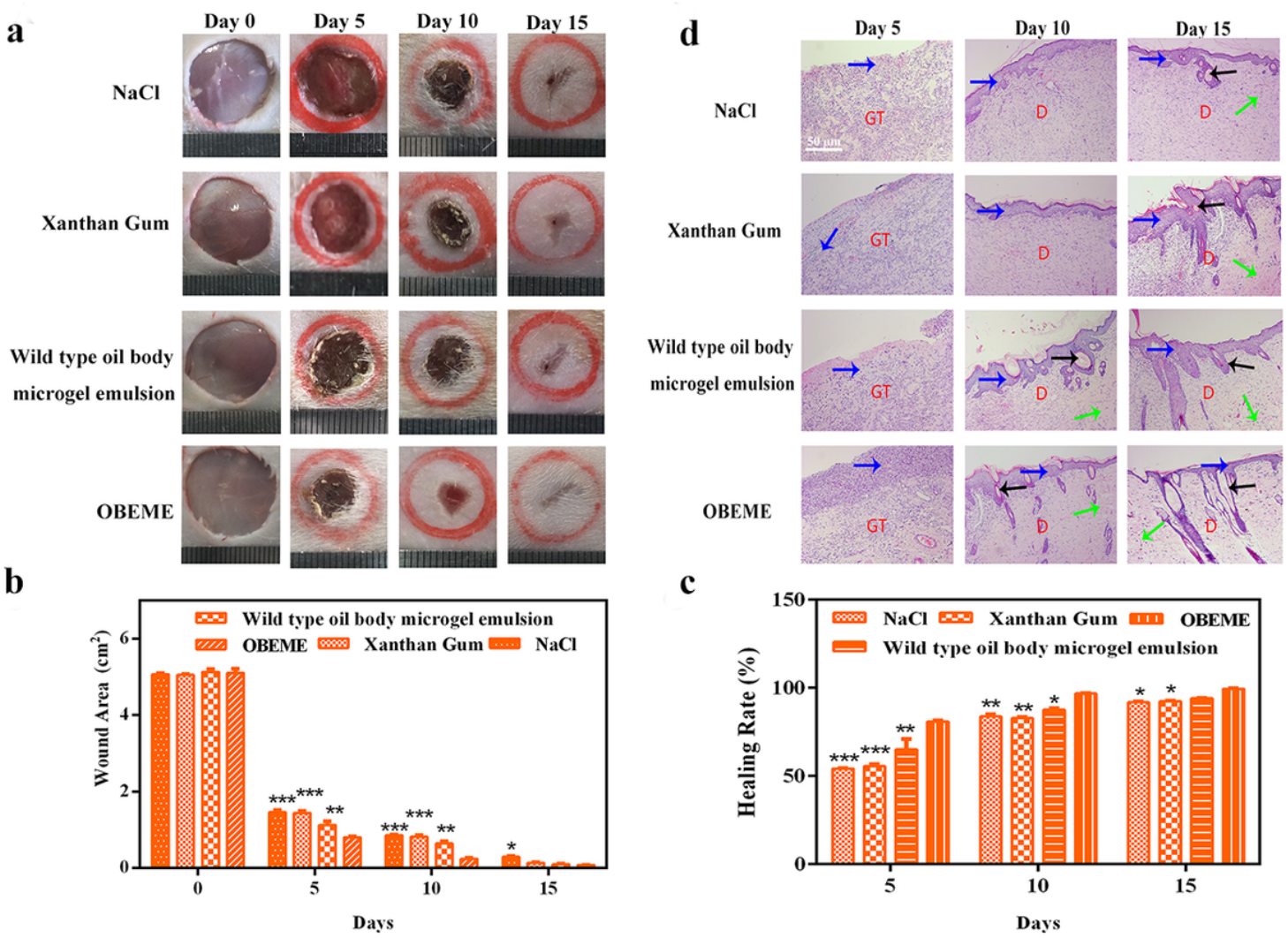

Figure 4

The ability of wound healing from the OBEME. **a** The photos of wound closure; **b** Statistics of wound area; **c** Statistics of wound healing rates; **d** Hematoxylin and Eosin analysis for different groups in wound healing. *p<0.05, **p<0.01, ***p<0.001 (n=3) unpaired one-way ANOVA multiple test was used in analyses. bar: 50 μm. (GT: granulation tissue; D: Newly formed dermis; Blue arrow: Newly formed epidermis; Black arrow: Newly formed hair; Green arrow: Newly collagen)

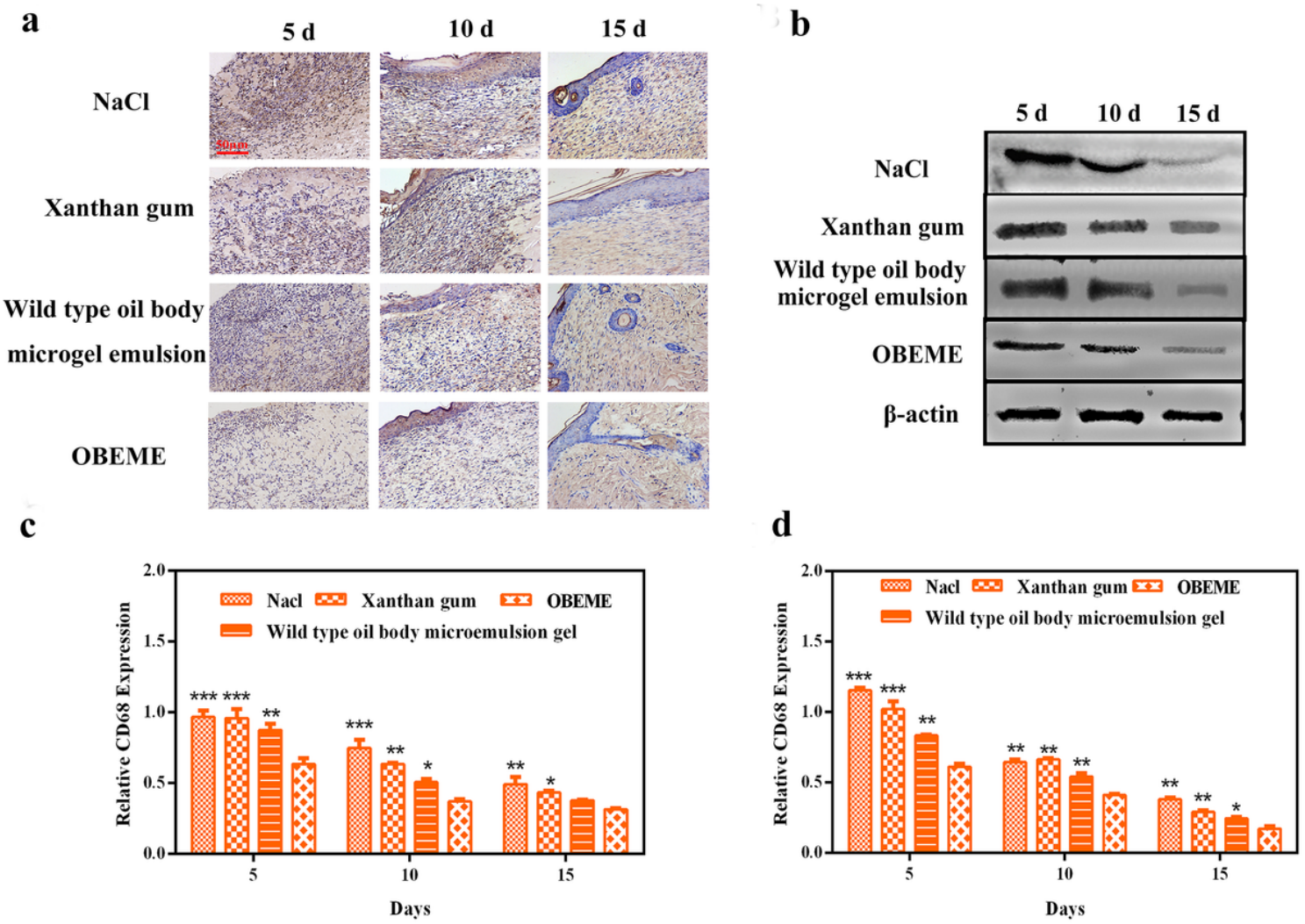

Figure 5

Protein expression of CD68 measured with immunostaining and western blot. **a** Immunostaining of CD68; **b** Western blot of CD68 in wound section on days 5, 10 and 15. **c** Statistical analysis of CD68 measured with immunohistochemistry; **d** Statistical analysis of CD68 expression measured with Western blot. *p<0.05, **p<0.01, ***p<0.001 (n=3) unpaired one-way ANOVA multiple test was used in analyses. bar: 50 μm.

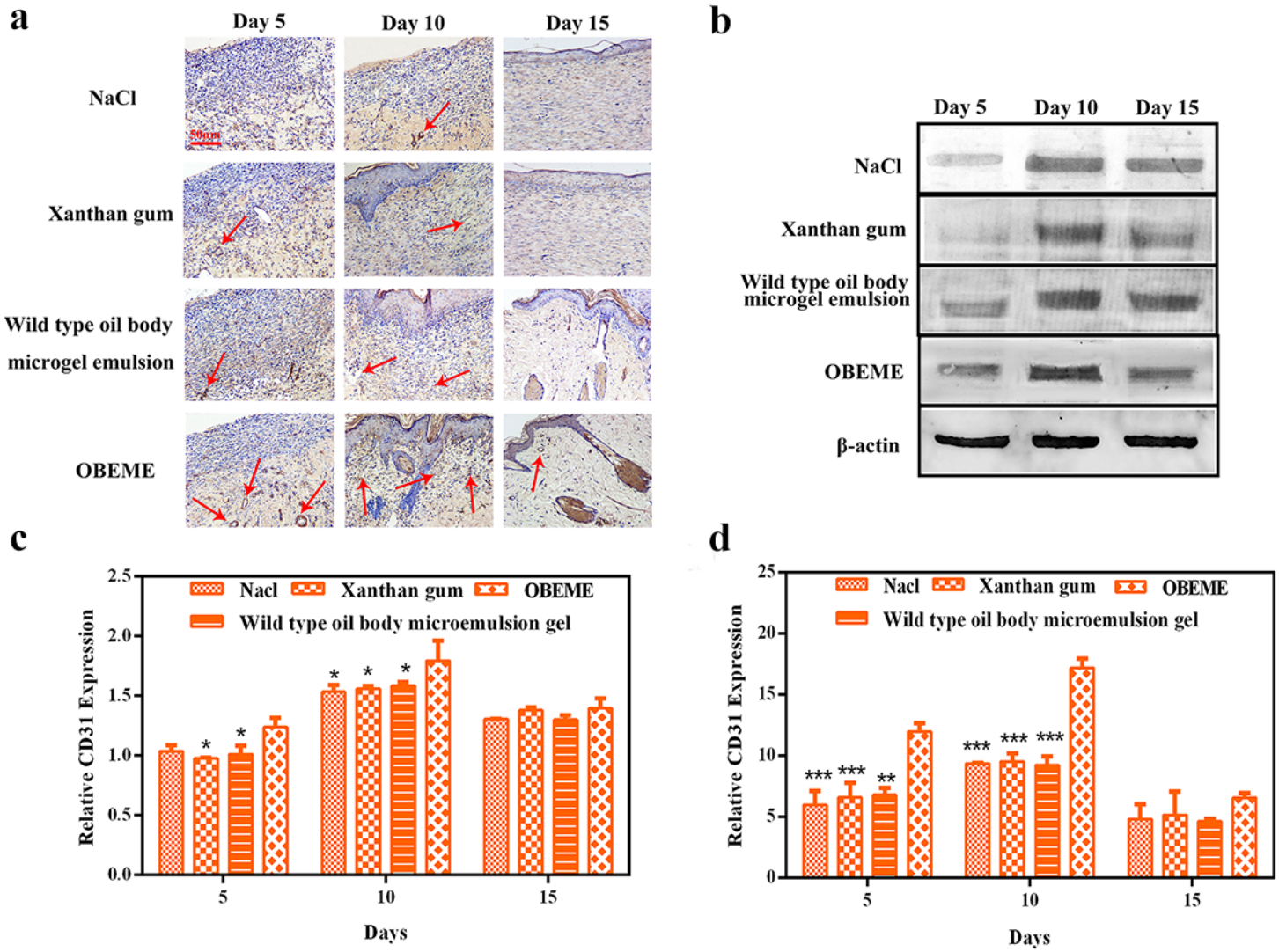

Figure 6

Protein expression of CD31. **a** Immunostaining of CD31; **b** Western blot of CD31 in wound section on days 5, 10 and 15; **c** Statistical analysis of CD31 measured with immunohistochemistry; **d** Statistical analysis of CD31 expression measured with Western blot. *p<0.05, **p<0.01, ***p<0.001 (n=3) unpaired one-way ANOVA multiple test was used in analyses. bar: 50 μm. (Red arrow: Newly blood vessels)

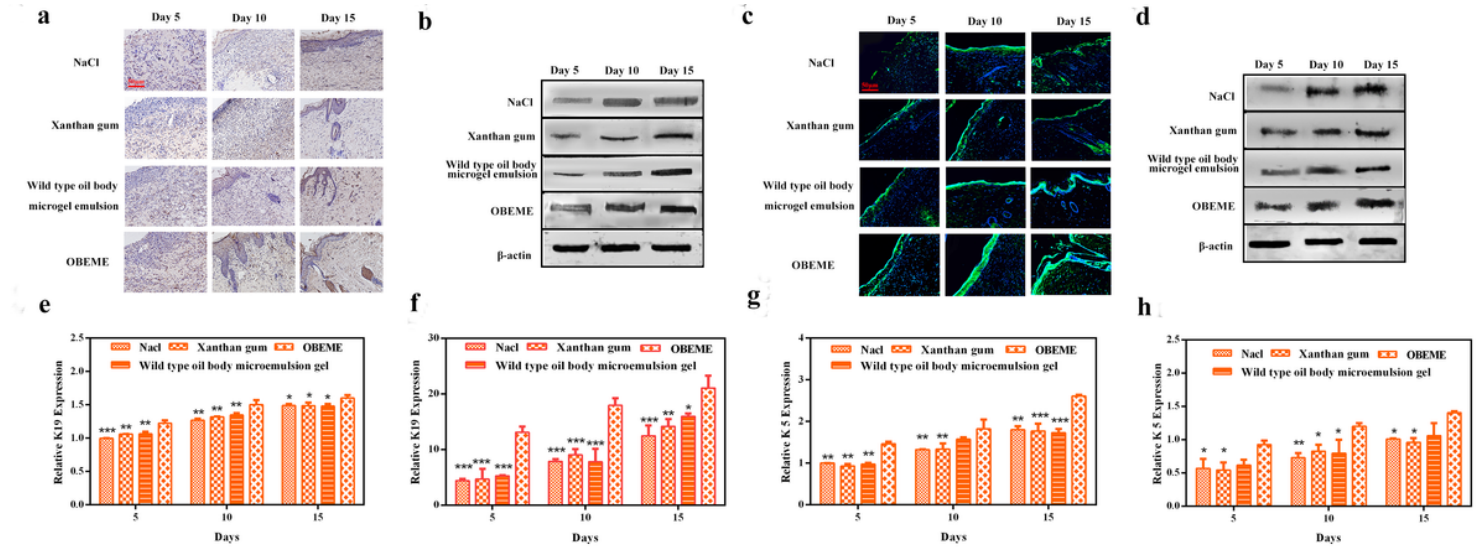

Figure 7

Protein expression of K19 and K5. **a** Immunostaining of K19; **b** Western blot of K19 in wound section on days 5, 10 and 15; **c** Immunofluorescence of K5 in epidermis on day 5, 10 and 15; **d** Western blot of K5 in wound section on days 5, 10 and 15; **e** Statistical analysis of K19 measured with immunohistochemistry; **f** Statistical analysis of K19 expression measured with Western blot; **g** Statistical analysis of K5 expression measured with immunofluorescence; **h** Statistical analysis of K5 expression measured with Western blot. *p<0.05, **p<0.01, ***p<0.001 (n=3) unpaired one-way ANOVA multiple test was used in analyses. bar: 50 μm.

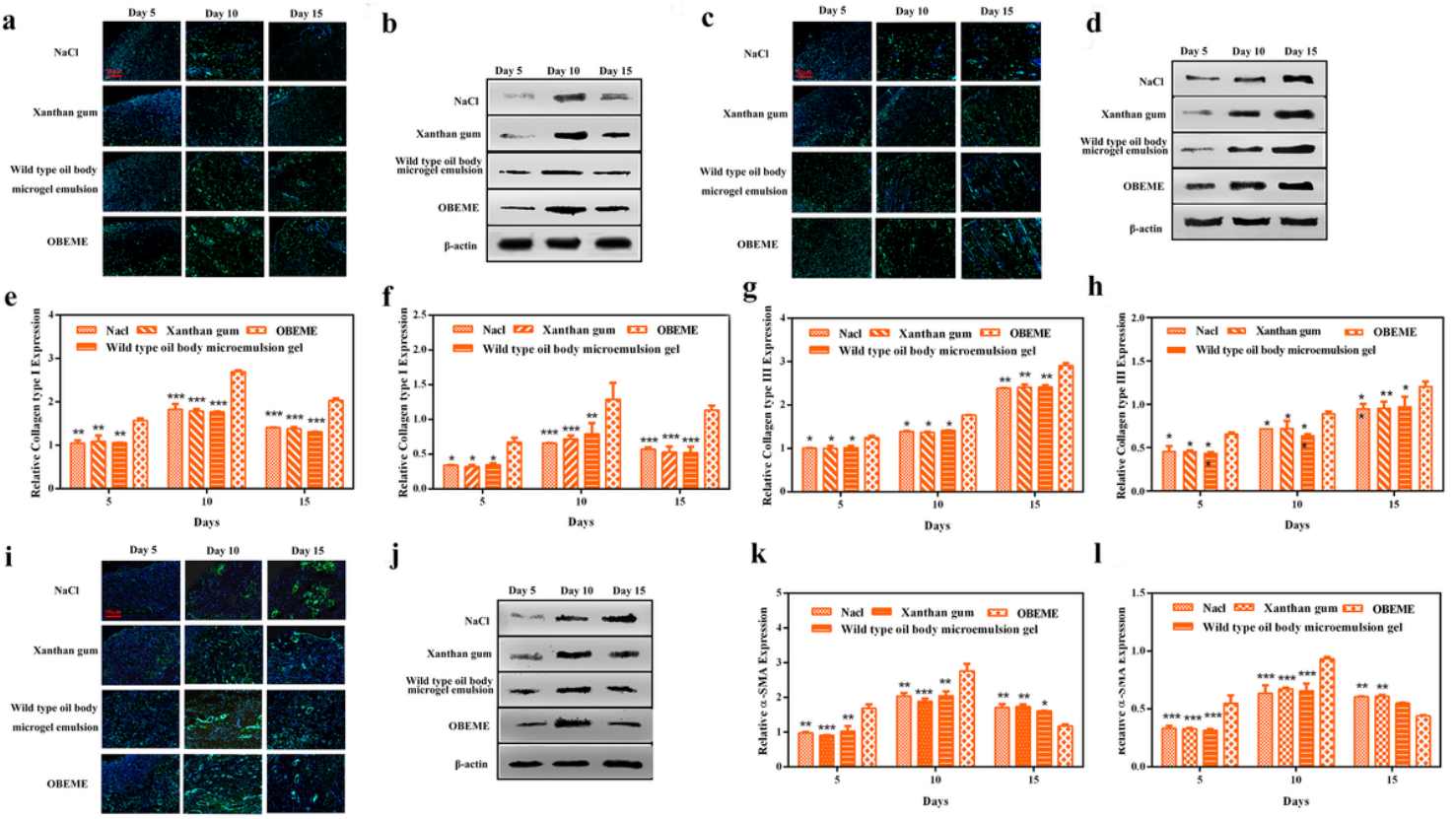

Figure 8

Protein expression of collagen I, collagen III and α-SMA. **a** Immunofluorescence of collagen I; **b** Western blot of collagen I in wound section; **c** Immunofluorescence of collagen III; **d** Western blot of collagen III in wound section; **e** Statistical analysis of collagen I with immunofluorescence; **f** Statistical analysis of collagen I expression with western blot; **g** Statistical analysis of collagen III with immunohistochemistry; **h** Statistical analysis of collagen III expression with western blot; **i** Immunofluorescence of α-SMA in dermis; **j** Western blot of α-SMA in wound section; **k** Statistical analysis of α-SMA expression with immunofluorescence; **l** Statistical analysis of α-SMA expression with western blot. *p<0.05, **p<0.01, ***p<0.001 (n=3) unpaired one-way ANOVA multiple test was used in analyses. bar: 50 μm.